Molecular dynamics study on the *Apo*- and *Holo*-forms of 5-lipoxygenase

Juan Torras [iD][1*]
Mauro Maccarrone [iD][2,3†]
Enrico Dainese [iD][3,4*,†]

[1]*Department of Chemical Engineering, Escola d'Enginyeria de Barcelona Est (EEBE), Universitat Politècnica de Catalunya, Barcelona, Spain*

[2]*Department of Medicine, Campus Bio-Medico University of Rome, Rome, Italy*

[3]*European Center for Brain Research (CERC)/Santa Lucia Foundation IRCCS, Rome, Italy*

[4]*Faculty of Bioscience and Technology for Food Agriculture and Environment, University of Teramo, Teramo, Italy*

Abstract

Lipoxygenases (LOXs) are nonheme iron-containing enzymes catalyzing the dioxygenation of polyunsaturated fatty acids. LOX catalytic activity depends on the presence of iron in the active site and the iron removal is also able to affect the membrane binding properties of the enzyme. Leukotrienes biosynthesis is initiated by the action of 5-LOX at the level of nuclear membrane and the mechanism of enzyme–membrane interaction is thought to involve structural flexibility and conformational changes at the level of the protein tertiary structure. In this study, we have analyzed by molecular dynamics simulations the conformational changes induced by iron removal in 5-LOX. The data indicate that the degree of enzyme flexibility is related to the presence of iron into the active site that is able to stabilize the protein increasing its rigidity. These findings provide further evidence that the conformation and the functional activity of LOXs is tuned by the presence of iron at the active site, suggesting new approaches for the design of enzyme inhibitors. © 2017 International Union of Biochemistry and Molecular Biology, Inc. Volume 00, Number 0, Pages 1–8, 2017

1. Introduction

The molecular dynamics (MD) that controls the biological function of a protein strictly depends on the fine balance between the external interactions of surface groups with the solvent and the intramolecular forces. In the structural and functional study of the protein–lipid interactions, cytosolic enzymes able to translocate to membranes in response to specific stimuli could play a pivotal role. An important group of cytosolic enzymes able to use lipids and biological membranes as substrates is the lipoxygenase (LOX) family. These proteins are nonheme, nonsulfur iron-containing enzymes, which catalyze the dioxygenation of polyunsaturated fatty acids containing one or more pentadiene systems to the corresponding hydroperoxy derivatives. The available crystal structures of LOXs indicate single polypeptide chain proteins adopting a two-domain folding: the N-terminal "C2-like" domain proposed to be involved in bringing the enzyme in proximity to its arachidonate substrate within the nuclear membranes [1] and the larger catalytic C-terminal domain, that is, primarily α-helical and harbors the nonheme catalytic iron [2].

Some mammalian LOXs are activated by a Ca^{2+}-mediated translocation from plasma membranes to nucleus upon cell stimulation [3], and the translocation of 5-LOX is assisted by a 5-LOX activating protein (FLAP) [4]. The amount of *apo*-form of the enzyme found has been previously documented in several mammalian cells [5, 6]. An approach to elucidate the structure–function relationship in metalloenzymes is the extraction, reconstitution, and substitution of the central coordinated metal [7, 8]. This methodology has not

been successful with some LOX enzymes but iron extraction from porcine leukocyte 12-LOX [9] and soybean LOX-3 [10] was reported. Also from the C-terminal fraction of soybean LOX-1 (miniLOX) [11] iron was removed and a partial activity recovery on the metal-reconstituted/substituted forms of miniLOX was obtained [12]. In particular, it was demonstrated that iron ion stabilizes the structure of LOX and its presence is also crucial for the membrane binding of the enzyme [12].

In this study, we evidenced by MD analysis that the presence of iron within the active site stabilizes the conformation of the human 5-LOX. These results are in line with previous data obtained with LOX-1 from soybean [12] and confirm a crucial role for iron in preserving the structural stability and membrane binding ability of the enzyme. The here reported conformational change between the *apo-* and *holo*-5-LOX might contribute *in vivo* to the 5-LOX trafficking among different compartments of the cell, thus leading to a modulation of its signaling.

2. Materials and Methods

2.1. Molecular models

All human 5-LOX models used in this work are based in the X-ray crystallographic structure of stable 5-LOX mutant human enzyme at 2.4 Å of resolution [2]. Specifically, 5-LOX $K^{653}K^{654}K^{655}$ amino acids from the human enzyme were replaced with the $E^{653}N^{654}L^{655}$ sequence (KKK→ENL substitution) to stabilize the enzyme. Stable-5-LOX is made of two similar chains containing each one two distinct domains: the N-terminal "C2-like" domain with about 120 amino acids and the larger catalytic domain, mainly alpha-helical (~550 amino acids). The latter is harboring the active site containing a nonheme catalytic iron (Fe^{2+}) coordinated by three histidines ($His^{367,372,550}$), as well as the main-chain carboxylate of the C terminus (Ile^{673}).

The simulated systems consisted of two different molecular structures built to model both the *holo*-form of stable 5-LOX enzyme and its *apo*-form, where the two iron metal atoms were removed from their active site. The *holo*- and *apo*-forms of 5-LOX enzyme model systems are made of the main protein solvated with 52,308 and 50,177 water molecules, respectively. TIP3P model was used to represent explicit water molecules [13].

2.2. Parameterization of the active site

The active site model, containing Fe^{2+} ion, was parameterized starting from stable crystal structure of 5-LOX to obtain the force field parameters. Figure 1b shows truncated structure of stable-5-LOX enzyme active site. The four amino acids lying on the first coordination sphere of iron were truncated to their most relevant parts; histidines and isoleucine are represented by ethyl imidazole rings and methyl-isoleucine, respectively. The parameters of the active site were obtained by means of the MCPB method developed by Peters and colleagues [14], which
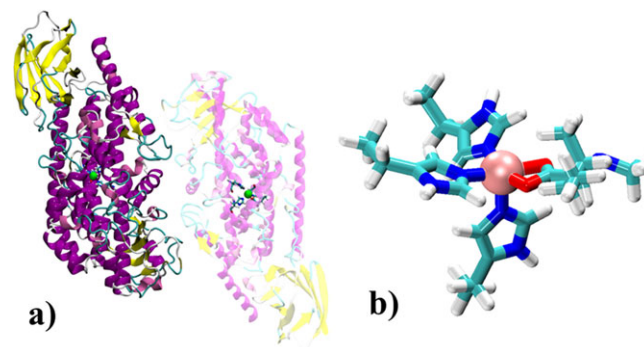

FIG. 1   *(a) Structural model of 5-LOX dimer with its active site highlighted in one of the enzyme monomers and (b) truncated model of the active site.*

is embedded into the MTK++ software package in AMBER 2016 [15]. MCPB is a semiautomatic method based on bonded models for representing the interactions between metal and its coordinating sphere of amino acids. Thus, bond, angle, and electrostatic terms were parametrized meanwhile dihedral terms were ignored under the assumption made by Hoops and colleagues [16] based on the rigidity of the metal ions geometry, which are devoid of any significant torsional rotation. More specifically, the active site model (Fig. 1b) was subjected to a quantum mechanical constrained geometry optimization in gas phase using Gaussian 03 [17] program at B3LYP/6-31G* level. Geometry parameters were derived from equilibrium values of bond lengths and angles involving Fe^{2+} and its coordination sphere of amino acids. Force constants were determined using the method described by Seminario [18] from submatrices of the Cartesian Hessian matrix. The atom-centered partial charges were derived using the restrained electrostatic potential (RESP) schemes [19] using a large active site model by capping each of the methyl groups with acetylamide and N-methylamide groups, and apply the same level of quantum mechanics (QM) calculation to derive the RESP charge parameters. Moreover, if Fe^{2+} ion is buried within the protein, then the Lennard-Jones parameters are not as important as the electrostatics [20], so those being taken from the literature [21]. The MCPB method has been widely used in previous studies to facilitate the modeling of metal effects of the metalloproteins [22–24].

2.3. MD protocol

Classical MD simulations were performed on both *holo*- and *apo*-forms of human 5-LOX enzyme using explicit solvent and periodic boundary conditions. The ff14SB AMBER force field [25] for the protein was applied and updated with previous active site parameterization values. The AMBER 2016 program [15] was used in all classical simulations. The system preparation and final production run have been the same for the two models. Initially, the system was equilibrated by keeping protein restrained to initial position using quadratic harmonic restraints with a constant force of 20 kcal mol^{-1} Å^{-2}. Each system was subjected to 2.5×10^4 minimization steps, using
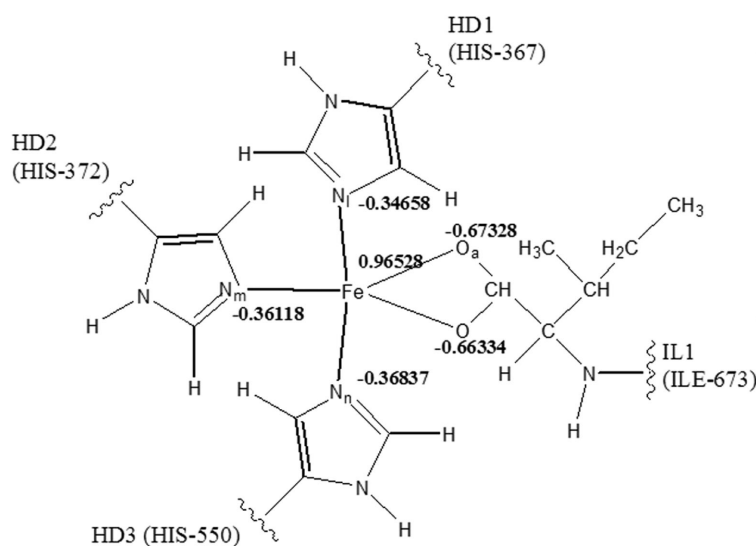
Bonds	K_b (kcal mol^{-1}Å^{-2})	R_e (Å)
Fe-N$_l$	88.06	1.972
Fe-N$_m$	103.14	1.925
Fe-N$_n$	94.43	1.960
Fe-O$_a$	81.61	2.001

Angles	K_θ (kcal mol^{-1}rad^{-2})	R_e (deg)
N$_m$-Fe-N$_n$	75.220	94.972
N$_m$-Fe-O$_a$	79.397	95.050
N$_l$-Fe-N$_m$	80.742	99.804
N$_l$-Fe-N$_n$	115.662	97.360
N$_l$-Fe-O$_a$	117.627	157.867
N$_n$-Fe-O$_a$	129.037	97.598

FIG. 2 Force field parameters of Fe^{2+} center in 5-LOX.

the MM Hamiltonian to remove any atomic contact, and then heated to 298 K for 60 pSec at constant volume. The numerical integration step was set to 2.0 fSec, and the Langevin thermostat was used with a 5.0 pSec^{-1} collision frequency. The system was allowed to relax for an additional 500 pSec using an NPT ensemble at 298 K and 1 atmosphere of pressure. In all cases, the bond lengths involving hydrogen atoms were kept at their equilibrium distance by means of the SHAKE algorithm [26]. Atom pair distance cutoffs were applied at 10.0 Å to compute the van der Waals interactions. Long-range electrostatics was computed by means of the particle mesh Ewald method [27]. The harmonic restraints on the solute atoms were released and an additional trajectory was obtained, up to constant density, under the same conditions previously described for 5 nSec. Finally, the production series were obtained using an NVT ensemble at 298 K for 100 nSec. The coordinates of production trajectories were saved at 20 pSec intervals for subsequent analysis.

3. Results and Discussion

### 3.1. Parameterization of the iron active site

The iron coordination sphere is very similar in most of the known LOX structures [3], adopting a pseudooctahedral geometry [28]. A remarkable feature of the coordination sphere in this enzyme is the utilization of the main chain carboxy-terminus as an iron ligand. The iron cluster optimization of 5-LOX active site, performed using the MCPB method, leads to a similar structure to the crystallographic data but the carboxylate moiety of Ile[673] is presented as a bidentate ligand with a bond distance of 2.001 Å (Fig. 1). A sketch of the new

parameterization for the first amino acid coordination sphere is shown in Fig. 2 (all the parameters are listed in the Supporting Information). A shorter bond distance ($\Delta d \sim 0.15$–0.25 Å) between the metallic ion and the ligands is derived from iron cluster optimization and compared with crystallographic data. Moreover, a charge reorganization on the iron ligands is observed with a resulting positive partial charge of +0.975 a.u. for the Fe^{2+}, meanwhile the three His and Ile residues, in direct contact with iron, are holding a partial charge ranging from –0.347 to –0.673 a.u., respectively.

We performed 100 nSec explicit water MD simulations in order to differentiate the behavior between the *apo-* and the *holo*-forms of 5-LOX systems. Initially, the root mean standard deviation (RMSD) of all the protein backbone atoms in both systems was obtained in order to monitor the protein structure fluctuations from initial structure (see Fig. 3). Both systems reached their equilibria very quickly, and after 20 nSec no much large fluctuations were observed. Thus, in the absence of Fe^{2+} ion, the stability is not apparently different from that of *holo*-form of 5-LOX system. However, when the RMSD of the atoms belonging only to the first amino acid sphere that are linked to the iron center is considered (see Fig. 3), a large conformational differences in the *apo*-form are observed and compared with the RMSD graph of the *holo*-form of 5-LOX protein. Then, the impact of metal removal in the system will be studied in this work.

3.2. Interdomain motion

Hammel and colleagues [29] reported a high degree of motional freedom of the N-terminal β-barrel domain of 15-LOX in aqueous solutions, which might be of importance for regulation of the catalytic activity and membrane binding. These observations were based on a bigger molecular volume of the N-terminal β-barrel domain and on a bending of the enzyme molecule in solution that was not observed in the

a)

b)
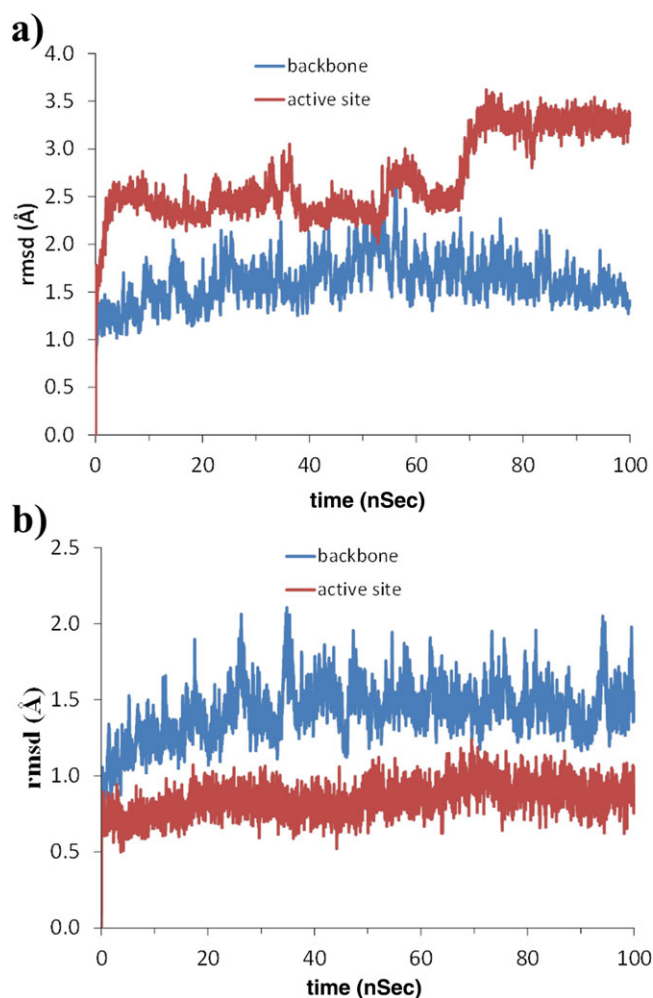
FIG. 3 *Root mean square deviation of backbone atoms
(blue line) and active site atoms (brown line) of
5-LOX dimer from the initial structures of the
enzyme (a) without iron content (apo-form of
5-LOX) and (b) with iron content (holo-form of
stable 5-LOX).*

crystal structure. The interdomain motion differences between *apo*- and *holo*-5-LOX proteins was verified by the evaluation of the bending and movement study on the N-terminal domain by considering the unstructured stretch of amino acids 111–119 (random coil) as an interdomain linker. Therefore, three averaged parameters were extracted from the whole MD trajectory to explore such motion between domains: the distance between the center of mass of N-terminal domain and the center of mass of C-terminal domain of 5-LOX protein ($d^{CM}_{NC\text{-Domain}}$), the distance between N-terminal and C-terminal of 5-LOX protein ($d^{ee}_{NC\text{-Domain}}$), and the bending angle between the center of mass of N-terminal domain (residues 1–110) to the center of mass of interdomain linker (residues 111–119) to the center of mass of C-terminal domain (residues 120–669), denoted as $\alpha^{CM}_{NC\text{-Domain}}$. Table 1 lists the averaged values derived from MD trajectory, and Fig. 4 shows the fluctuation in the central bending of both solvated 5-LOX systems. There is no significant difference for the distances between the centers of mass of N-terminal and C-terminal domains of both *apo*- and *holo*-forms. Also, the end-to-end distances between domains are slightly different possibly due to the flexibility that presents the C-terminal on the *apo*-form, which is not being linked to the central coordination metal ion. Thus, no appreciable linear movement of the entire N-terminal β-barrel domain going away from the catalytic subunit was observed during in-solvent simulation of both systems. However, a slight difference of 1.6 Å was obtained in the $d^{ee}_{NC\text{-Domain}}$ distance between both forms.

On the other hand, the bending angle observed between the two domains within each 5-LOX monomer is around 85.6° and 85.3° for the *apo*- and the *holo*-forms, respectively. A slight difference of about half degree is obtained with a more pronounced and less dispersed frequency of occurrences from the interdomain angle distribution on the *holo*-form of stable-5-LOX protein. Similarly, calculated root mean square fluctuations of backbone atoms, averaged over the last 50 nSec of simulation (not shown), present a little larger deviations for the residues of β-barrel domain, showing thus an *apo*-form a little more flexible than the *holo*-form. The bending on the β-barrel domain, articulated by a random coil section, leads

**TABLE 1** *Averaged interdomain motion values between N-terminal and C-terminal domains. Values derived from apo- and holo-forms of 5-LOX MD trajectories. Standard error of the mean is also shown.*

	apo-5-LOX			holo-5-LOX		
	mon A[a]	mon B[b]	dimer	mon A[a]	mon B[b]	dimer
$d^{CM}_{NC\text{-Domain}}$ (Å)	42.4 ± 0.0	42.1 ± 0.0	42.3 ± 0.0	42.4 ± 0.0	42.8 ± 0.0	42.6 ± 0.0
$d^{ee}_{NC\text{-Domain}}$ (Å)	47.5 ± 0.0	48.8 ± 0.1	48.2 ± 0.1	48.9 ± 0.0	50.6 ± 0.0	49.8 ± 0.1
$\alpha^{CM}_{NC\text{-Domain}}$ (°)	86.1 ± 0.1	85.2 ± 0.0	85.6 ± 0.1	84.8 ± 0.0	85.8 ± 0.0	85.3 ± 0.1

[a]Monomer A from 3O8Y PDB file;

[b]Monomer B from 3O8Y PDB file

Values derived from *apo*- and *holo*-forms of 5-LOX MD trajectories. Standard error of the mean is also shown.

a)

b)
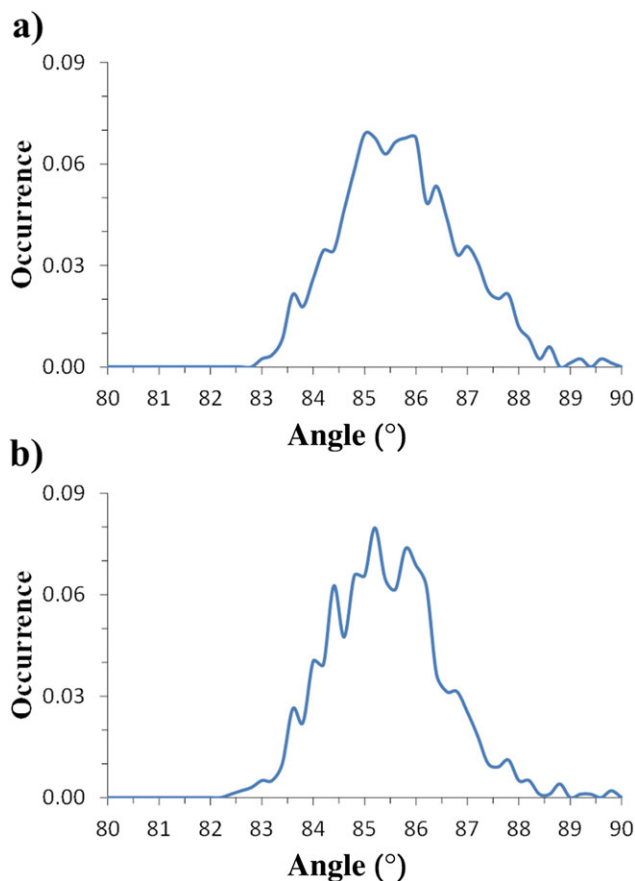
FIG. 4 Histogram analysis of the angle between N-terminal and C-terminal catalytic domain ($\alpha^{CM}{}_{NC\text{-}Domain}$) of (a) apo-form and (b) holo-form of 5-LOX.

to stretching of the enzyme molecule but may also induce a bending of the overall shape.

3.3. Solvent accessible surface

Protein–protein interfaces can be defined based on the change in their solvent accessible surface (SAS) on a dimerization process [30]. SAS is a measure typically used to quantify the degree to which the solvent can interact with different parts of the protein. In this work, the ΔSAS will be used to determine the protein–protein interface extension between both monomers of the 5-LOX dimer (ΔSAS$_{\text{Intf-dim}}$), and the domain–domain interface extension between the N-terminal domain and the catalytic C-terminal domain in both monomers (ΔSAS$_{\text{Intf-NCmonA}}$ and ΔSAS$_{\text{Intf-NCmonB}}$) defined as follows:

$$\Delta\text{SAS}_{\text{Intf}-\text{dim}} = {}^{1}/_{2}\left(\text{SAS}_{\text{monA}} + \text{SAS}_{\text{monB}} - \text{SAS}_{\text{dimer}}\right)$$
$$\Delta\text{SAS}_{\text{Intf}-\text{NCmonA}} = {}^{1}/_{2}\left(\text{SAS}_{\text{Nterm\_monA}} + \text{SAS}_{\text{Cterm}-\text{monA}} - \text{SAS}_{\text{monA}}\right),$$
$$\Delta\text{SAS}_{\text{Intf}-\text{NCmonB}} = {}^{1}/_{2}\left(\text{SAS}_{\text{Nterm\_monB}} + \text{SAS}_{\text{Cterm}-\text{monB}} - \text{SAS}_{\text{monB}}\right)$$

$$(1)$$

where the N-terminal domain are defined by residues 1 up to 114 and C-terminal domain from residue 115 up to 669.

TABLE 2 Averaged accessible surface area (Å^2, SAS) buried within the interface of the dimer and the interface between N-terminal and C-terminal domains. Values derived from apo- and holo-forms of 5-LOX MD trajectories. Standard error of the mean is also shown.

	apo-5-LOX	holo-5-LOX
SAS$_{\text{Intf-dim}}$	$1{,}134 \pm 3$	$1{,}133 \pm 4$
SAS$_{\text{Intf-NCmonA}}$	$1{,}268 \pm 2$	$1{,}285 \pm 3$
SAS$_{\text{Intf-NCmonB}}$	$1{,}100 \pm 3$	$1{,}113 \pm 3$

Values derived from apo- and holo-forms of 5-LOX MD trajectories. Standard error of the mean is also shown.

Comparison of average ΔSAS on the apo- and holo-forms of stable 5-LOX systems computed from MD simulation results (last 50 nSec) are listed in Table 2. The absence of Fe^{2+} ion does not lead to any important difference in the buried surface of stable 5-LOX dimer, with values of 1134 Å^2 (~4.1 % of the total solvent accessible area of each monomer). However, N-terminal β-barrel domain presents a lower buried surface in contact with the catalytic C-terminal domain in the apo-form (~1.2% decrease in the buried surface), suggesting a bit larger interdomain motion when is compared with the holo-form. This result is qualitatively consistent with previous section when a little more flexible apo-form was observed.

3.4. Clustering analysis

A different time evolution of conformations on the coordination sphere of amino acids linked to the Fe^{2+} ion in the apo-form has been previously observed (Fig. 3). In this section, a more detailed study on the structural difference between the active site of apo- and holo-forms of stable 5-LOX enzyme is performed by means of clustering analysis. The well-known density-based spatial clustering analysis with noise algorithm, which classifies particles in the MD snapshot into clusters based on particle density variations, was used to group similar structures [31]. The postprocessing of trajectories was carried out using the cpptraj program from the AMBER 2016 package [15].

The metrics used to obtain ligand dispersion measurement between amino acids in the coordination sphere of Fe^{2+} ion is the one-to-all averaged distance between their atom ligands (d_{as}, Eq. (2)):

$$d_{\text{as}} = \frac{1}{3}\left(d_{\text{His372@N}-\text{His550@N}} + d_{\text{His372@N}-\text{His367@N}} + d_{\text{His372@N}-\text{Ile673@O}}\right)$$

$$(2)$$

Table 3 lists d_{as} distance for the most populated representative clusters. The holo-form of stable- 5-LOX system presents a pseudooctahedral geometry with a d_{as} value of ~3 Å. However, the highly populated cluster representatives of apo-form presents a much large d_{as} value with a range of

TABLE 3 — *Population of cluster representatives as a fractional value (χ, only populations higher than 5%) and averaged distance between atom–ligands (d_{as} in Å) from apo- and holo-forms of 5-LOX MD trajectories*

| | apo-5-LOX | | | | holo-5-LOX | | | |
| | AS1 | | AS2 | | AS1 | | AS2 | |
Cluster	χ	d_{as}	χ	d_{as}	χ	d_{as}	χ	d_{as}
c_0	0.620	6.34	0.541	6.42	0.970	2.98	0.694	3.08
c_1	0.362	7.29	0.120	6.41	0.021	3.06	0.296	2.94
c_2			0.108	6.94				
c_3			0.055	6.40				

distances between ~6.3 up to ~7.3 Å. A close inspection to the cluster representatives (Fig. 5) shows some dispersion, mainly located on the carboxylic moiety of the Ile[673] residue due its easy mobility as a C-terminal residue. The three His residues do not suffer such a large dispersion due to a general structural stability observed during in-solution simulation of the *apo*-form but there is an appreciable increase between nitrogen–ligand atoms distances.

Fuchs and colleagues [32] reported that the release of iron ions on some LOX-catalyzed transformations might be caused by modifications of histidine residues located at the active site of the enzyme. The presence of three labile histidines on the LOX enzyme may be affected by active site modifications and thus causing iron release and LOX inactivation [33]. In fact, the importance of the three histidines of 5-LOX active site was previously reported by Zhang and colleagues [34], determining that His[372] and His[550] constitute two of the iron ligands in 5-LOX as well as the necessity of His[367] presence for the enzyme activity, although the latter residue is not crucial for iron binding. The distance between nitrogen–ligand atoms of His[372] and His[550], on the representative structure of the most populated cluster, rises from 2.92 Å up to 4.83 Å for the *as1* of *holo-* and *apo*-forms, respectively, when iron ion is removed from the active site. The observed dispersion on the two main iron ligands might explain the difficult to recovery 5-LOX activity when the *apo*-form is reconstituted with the lost iron metal center [9, 10, 12].

3.5. Closest waters
The presence of water molecules in the coordination sphere of Fe^{2+} ion in the LOX active site is believed to play an important role in the catalytic mechanism of LOX in its active Fe^{3+} form [35]. However, water molecules in 5-LOX are not so tightly coordinated to the iron such as the 12-LOX with 2.2 Å of coordination distance reported from X-ray structure [36]. Indeed, crystallographic structure of 5-LOX [2] shows one coordination distance of 3.6 Å in monomer **A** only, and no coordination in monomer **B** (first water at 5.75 Å), meanwhile
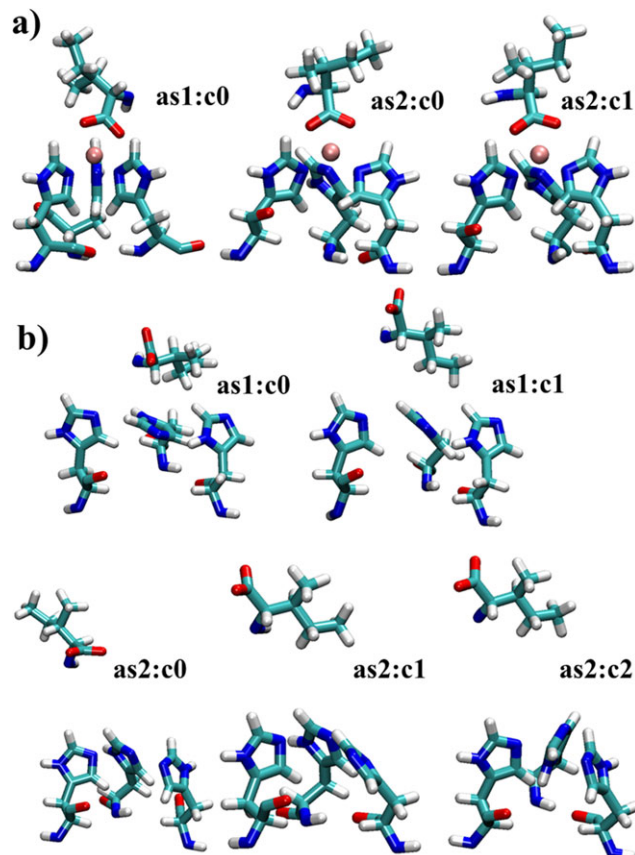
FIG. 5 — *(a) Representative cluster conformations of holo-form of 5-LOX with a population higher than 5% at 298 K during the last 50 nSec of simulation. Representative examples of each active site (as₁ and as₂) are shown. (b) Representative cluster conformations of apo-form 5-LOX with a population higher than 10% at 298 K during the last 50 nSec of simulation. Representative examples of each active site (as₁ and as₂) are shown.*

15-LOX enzyme does not presents water coordination with the first water being at 5.8 Å from the Fe^{2+} ion. Xu and colleagues [36] pointed that the structures of the iron sites in different LOX enzymes can be very different, which in turn might reinforce the notion that the potential flexibility of the iron ion and its coordination sphere structure could be relevant to catalysis. This latter observation was based on the observed rearrangement in the coordination sphere of the nonheme iron atom in the activation process [37].

In this work, water molecule presence in the coordination sphere of Fe^{2+} ion was explored by means of radial distribution function (RDF), evaluated for the Fe^{2+} ion and oxygen atom of water molecules depicted in Fig. 6. Attending to the different water location observed from crystallographic data, two different g_{Fe-O} RDF plots were derived, one at each monomer active site. The g_{Fe-O} RDF of monomer **A** (*as1*, Fig. 6a) shows a first peak at 4.05 Å and a second peak at 5.25 Å. Integration of the RDF (running number $n(r)$) up to first peak corresponds to 0.5
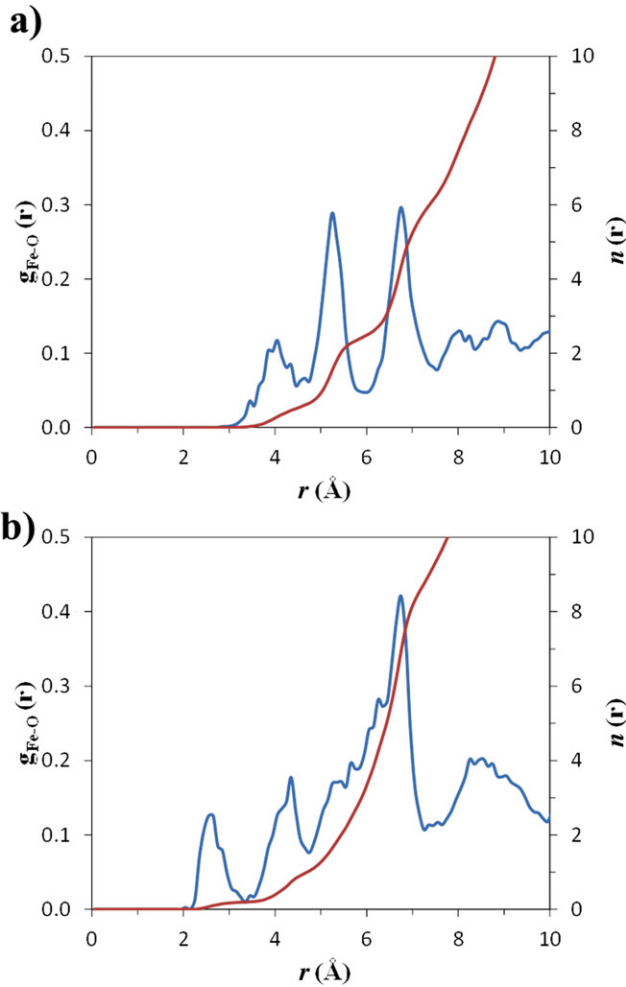
FIG. 6 *Radial distribution function between Fe^{2+} and oxygen atoms of water molecules (blue line) on the two active sites of 5-LOX (as_1 on the left and as_2 on the right). Running number of water molecules is also shown (brown line).*

water molecules bounded to Fe^{2+} ion and 2.5 water molecules up to the second peak. On the other hand, monomer **B** (*as2*, Fig. 6b) shows a first peak at 2.60 Å and a second peak at 4.35 Å with 0.2 and 1.0 water molecules in average bounded to metallic ion during MD trajectory for the first and second peak, respectively. This result agrees qualitatively with the crystallographic data, showing similar differences in the coordination distances of water between both monomeric units of 5-LOX. However, dynamical simulation in-solution of dimeric enzyme leads to a closer location of water molecules to the active sites ($\sim$4.0–4.3 Å) than those reported from crystallographic data. Moreover, some water molecules were found to be, with a mean distance of 2.6 Å, tightly coordinated with iron ion that might be precursor of activation process of the enzyme. This value corresponds to an intermediate distance between Fe^{2+} and its coordinated water observed in 12-LOX (2.2 Å) and 5-LOX (3.6 Å) [36].

4. Conclusions

In this paper, we studied the impact of Fe^{2+} ion on stable 5-LOX enzyme structure using comparative MD simulation between the *holo-* and *apo-*forms, obtaining the latter after removal of central iron. The force field parameters of Fe^{2+} were calculated by the MCPB method to obtain 100 nSec of MD trajectory. System dynamics shows a similar RMSD evolution for the backbone atoms of the protein on the two simulated systems, with differences mainly located on the amino acid coordination sphere where the *apo-*form presented a much more dispersive behavior.

The motional flexibility of the N-terminal β-barrel domain was verified by the central bending of LOX in solution. The overall dynamics showed a slightly different half degree, with a more pronounced and less dispersed frequency of the interdomain angle distribution of *holo-*form. The SAS study also corroborates this observation, thus suggesting a larger interdomain motion in the *apo-*form when compared with the *holo-*form. However, these data do not support the large conformational change previously suggested by Hammel and colleagues in mammalian 15-LOX [29]. Rather, the 5-LOX conformational flexibility reported here appears more in line with previous data demonstrating an increased rigidity of plant and a mammalian LOX protein when inhibitors are present in their active site, paralleled by impaired membrane binding ability [38].

Cluster analysis of the *holo-* and *apo-*5-LOX enzyme active sites shows an appreciable dispersion on the *apo-*form active site, mainly located on the carboxylic moiety of the C-terminal residue, Ile[673]. Moreover, the distance between nitrogen–ligand atoms of His[372] and His[550] within the active site increases about 2 Å when iron ion is removed, which might cause a conformational change that leads to different membrane binding properties of the *apo-*form.

Analysis on the water population dynamics nearby the *holo-*form active site showed a closer distance to the active sites in average than those reported on crystallographic data. In fact, in some cases it was observed water molecules tightly coordinated with iron ion that might act as a precursor of activation process of the enzyme.

In a site-directed mutagenesis study aimed at investigating the intracellular distribution of 5-LOX, it has been observed that mutations known to abolish enzyme activity, but leaving (at least in part) iron in the active site, induced a graded distribution of 5-LOX in the nucleus and cytosol, depending on the iron content [39]. We already provide evidence that the presence of iron within the active site stabilizes a conformation of LOX more suitable for the association with model membranes [12] and the here reported MD results seem to confirm a crucial role for iron in preserving the structural stability and membrane binding ability of the enzyme. Being the presence of an *apo-*form of the enzyme previously documented in several mammalian cells, this might eventually contribute *in vivo* to the 5-LOX trafficking among different compartments of the cell, and hence

modulating signaling thereof. A typical pathological feature of Alzheimer's disease (AD) is the appearance in the brain of senile plaques, made up of aggregates of misfolded β-amyloid, associated with an abnormal accumulation of some metal ions, including iron [40]. In this context, we have recently shown an increase in 5-LOX mRNA and protein levels, as well as enzyme activity, in late onset AD subjects compared to healthy controls [41], and consistently, here we show a significant role of iron in the structural and functional stabilization of 5-LOX. Thus, here we are speculating that our *in silico* structural results could be of relevance for the role of LOXs in inflammatory diseases and neurodegeneration with altered iron homeostasis, but also in neurodegeneration such as AD, where the activity of 5-LOX is indeed remarkably increased [42].

5. Acknowledgements

7. References

[1] Kulkarni, S., Das, S., Funk, C. D., Murray, D., and Cho, W. (2002) J. Biol. Chem. 277, 13167–13174.

[2] Gilbert, N. C., Bartlett, S. G., Waight, M. T., Neau, D. B., Boeglin, W. E., Brash, A. R., and Newcomer, M. E. (2011) Science 331, 217–219.

[3] Newcomer, M. E., and Brash, A. R. (2015) Protein Sci. 24, 298–309.

[4] Gerstmeier, J., Newcomer, M. E., Dennhardt, S., Romp, E., Fischer, J., Werz, O., and Garscha, U. (2016) FASEB J. 30, 1892–1900.

[5] Wecksler, A. T., Kenyon, V., Garcia, N. K., Deschamps, J. D., van der Donk, W. A., and Holman, T. R. (2009) Biochemistry 48, 8721–8730.

[6] Segraves, E. N., and Holman, T. R. (2003) Biochemistry 42, 5236–5243.

[7] Vachette, P., Dainese, E., Vasyliev, V. B., Di Muro, P., Beltramini, M., Svergun, D. I., De Filippis, V., and Salvato, B. (2002) J. Biol. Chem. 277, 40823–40831.

[8] van der Donk, W. A., Tsai, A.-L., and Kulmacz, R. J. (2002) Biochemistry 41, 15451–15458.

[9] Matsuda, S., Suzuki, H., Yoshimoto, T., Yamamoto, S., and Miyatake, A. (1991) BBA-Lipid Lipid Met. 1084, 202–204.

[10] Kariapper, M. S. T., Dunham, W. R., and Funk, M. O. (2001) Biochem. Biophys. Res. Commun. 284, 563–567.

[11] Maccarone, M., Salucci, M. L., van Zadelhoff, G., Malatesta, F., Veldink, G., Vliegenthart, J. F. G., and Finazzi-Agrò, A. (2001) Biochemistry 40, 6819–6827.

[12] Dainese, E., Angelucci, C. B., Sabatucci, A., De Filippis, V., Mei, G., and Maccarone, M. (2010) FASEB J. 24, 1725–1736.

[13] Jorgensen, W. L., Chandrasekhar, J., Madura, J. D., Impey, R. W., and Klein, M. L. (1983) J. Chem. Phys. 79, 926–935.

[14] Peters, M. B., Yang, Y., Wang, B., Füsti-Molnár, L., Weaver, M. N., Merz, K. M. (2010) J. Chem. Theory Comput. 6, 2935–2947.

[15] Case, D. A., Betz, R. M., Cerutti, D. S., Cheatham III T. E., Darden, T. A., Duke, R. E., Giese, T. J., Gohlke, H., Goetz, A. W., Homeyer, N., Izadi, S., Janowski, P., Kaus, J., Kovalenko, A., Lee, T. S., LeGrand, S., Li, P., Lin, C., Luchko, T., Luo, R., Madej, B., Mermelstein, D., Merz, K. M., Monard, G., Nguyen, H., Nguyen, H. T., Omelyan, I., Onufriev, A., Roe, D. R., Roitberg, A., Sagui, C., Simmerling, C. L., Botello-Smith, W. M., Swails, J., Walker, R. C., Wang, J., Wolf, R. M., Wu, X., Xiao, L., and Kollman, P. A., (2016) AMBER 2016, University of California, San Francisco, CA.

[16] Hoops, S. C., Anderson, K. W., and Merz, K. M. (1991) J. Am. Chem. Soc. 113, 8262–8270.

[17] Frisch, M. J., Trucks, G. W., Schlegel, H. B., Scuseria, G. E., Robb, M. A., Cheeseman, J. R., Montgomery, J. A. J., Vreven, T., Kudin, K. N., Burant, J. C., Millam, J. M., Iyengar, S. S., Tomasi, J., Barone, V., Mennucci, B., Cossi, M., Scalmani, G., Rega, N., Petersson, G. A., Nakatsuji, H., Hada, M., Ehara, M., Toyota, K., Fukuda, R., Hasegawa, J., Ishida, M., Nakajima, T., Honda, Y., Kitao, O., Nakai, H., Klene, M., Li, X., Knox, J. E., Hratchian, H. P., Cross, J. B., Bakken, V., Adamo, C., Jaramillo, J., Gomperts, R., Stratmann, R. E., Yazyev, O., Austin, A. J., Cammi, R., Pomelli, C., Ochterski, J. W., Ayala, P. Y., Morokuma, K., Voth, G. A., Salvador, P., Dannenberg, J. J., Zakrzewski, V. G., Dapprich, S., Daniels, A. D., Strain, M. C., Farkas, O., Malick, D. K., Rabuck, A. D., Raghavachari, K., Foresman, J. B., Ortiz, J. V., Cui, Q., Baboul, A. G., Clifford, S., Cioslowski, J., Stefanov, B. B., Liu, G., Liashenko, A., Piskorz, P., Komaromi, I., Martin, R. L., Fox, D. J., Keith, T., Al-Laham, M. A., Peng, C. Y., Nanayakkara, A., Challacombe, M., Gill, P. M. W., Johnson, B., Chen, W., Wong, M. W., and Gonzalez, C., Pople, J. A., (2004) Gaussian 03, Revision C.02, Gaussian, Inc., Wallingford, CT.

[18] Seminario, J. M. (1996) Int. J. Quantum Chem. 60, 1271–1277.

[19] Bayly, C. I., Cieplak, P., Cornell, W., and Kollman, P. A. (1993) J. Phys. Chem. 97, 10269–10280.

[20] Norrby, P.-O., and Brandt, P. (2001) Coord. Chem. Rev. 212, 79–109.

[21] Li, P., Roberts, B. P., Chakravorty, D. K., and Merz, K. M. (2013) J. Chem. Theory Comput. 9, 2733–2748.

[22] Tounge, B. A., and Reynolds, C. H. (2003) J. Med. Chem. 46, 2074–2082.

[23] Shi, H., Kang, B., and Lee, J. Y. (2014) J. Phys. Chem. B 118, 10355–10361.

[24] Hu, J., Hu, Z., Zhang, Y., Gou, X., Mu, Y., Wang, L., and Xie, X.-Q. (2016) J. Mol. Model. 22, 156.

[25] Hornak, V., Abel, R., Okur, A., Strockbine, B., Roitberg, A., and Simmerling, C. (2006) Proteins: Struct. Funct. Bioinf. 65, 712–725.

[26] Ryckaert, J.-P., Ciccotti, G., and Berendsen, H. J. C. (1977) J. Comput. Phys. 23, 327–341.

[27] Darden, T., York, D., and Pedersen, L. (1993) J. Chem. Phys. 98, 10089–10092.

[28] Gaffney, B. J. (1996) Annu. Rev. Biophys. Biomol. Struct. 25, 431–459.

[29] Hammel, M., Walther, M., Prassl, R., and Kuhn, H. (2004) J. Mol. Biol. 343, 917–929.

[30] Jones, S., and Thornton, J. M. (1996) Proc. Natl. Acad. Sci. 93, 13–20.

[31] Ester, M., Kriegel, H.-P., Sander, J., and Xu, X., (1996) A density-based algorithm for discovering clusters a density-based algorithm for discovering clusters in large spatial databases with noise. pp. 226–231, AAAI Press, Portland, OR.

[32] Fuchs, C., and Spiteller, G. (2000) Z. Naturforsch. C: J. Biosci. 55, 643.

[33] Percival, M. D. (1991) J. Biol. Chem. 266, 10058–10061.

[34] Zhang, Y. Y., Lind, B., Rådmark, O., and Samuelsson, B. (1993) J. Biol. Chem. 268, 2535–2541.

[35] Scarrow, R. C., Trimitsis, M. G., Buck, C. P., Grove, G. N., Cowling, R. A., and Nelson, M. J. (1994) Biochemistry 33, 15023–15035.

[36] Xu, S., Mueser, T. C., Marnett, L. J., and Funk, M. O., Jr. (2012) Structure 20, 1490–1497.

[37] Vahedi-Faridi, A., Brault, P.-A., Shah, P., Kim, Y.-W., Dunham, W. R., and Funk, M. O. (2004) J. Am. Chem. Soc. 126, 2006–2015.

[38] Di Venere, A., Nicolai, E., Ivanov, I., Dainese, E., Adel, S., Angelucci, B. C., Kuhn, H., Maccarrone, M., and Mei, G. (2014) Biochim. Biophys. Acta 1841, 1–10.

[39] Chen, X.-S., Zhang, Y.-Y., and Funk, C. D. (1998) J. Biol. Chem. 273, 31237–31244.

[40] Zecca, L., Youdim, M. B. H., Riederer, P., Connor, J. R., and Crichton, R. R. (2004) Nat. Rev. Neurosci. 5, 863–873.

[41] Di Francesco, A., Arosio, B., Gussago, C., Dainese, E., Mari, D., D'Addario, C., and Maccarrone, M. (2013) J. Alzheimers Dis. 37, 3–8.

[42] Chu, J., and Praticò, D. (2011) Am. J. Pathol. 178, 1762–1769.